JOC The Journal of Organic Chemistry

pubs.acs.org/joc Note

Steric Hindrance Favors σ Dimerization over π Dimerization for Julolidine Dicyanomethyl Radicals

Rui Zhang, Arkady Ellern, and Arthur H. Winter*

Cite This: J. Org. Chem. 2022, 87, 1507−1511 Read Online

ACCESS | Metrics & More | Article Recommendations | Supporting Information

ABSTRACT: Metastable radicals exist in a steady-state equilibrium in solution with dimers, which can be either σ dimers or π dimers. Here, we show that steric hindrance at the *para* position causes julolidine-derived dicyanomethyl radicals to form σ dimers rather than π dimers, the opposite behavior as seen in other carbon-centered radicals, where steric hindrance typically favors pimerization. The change in dimerization mode can be attributed to weaker London dispersion forces and a decreased orbital overlap in the sterically hindered dicyanomethyl radical π dimers, while the bulky groups exert relatively little effect on the energy of the σ dimer.

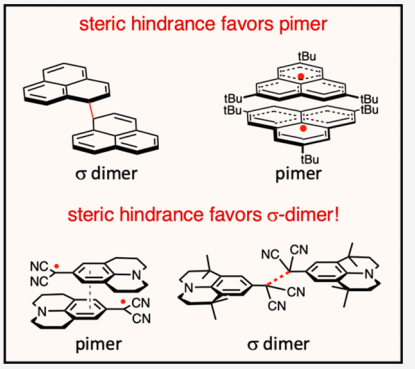

Free radicals that exist in equilibrium with dimers are useful building blocks for stimuli-responsive materials,[1−5] spin crossover materials,[6,7] and dynamic covalent assemblies.[3,4,8−10] Such metastable radicals dimerize to form either weak σ dimers or π dimers (pimers).[11−16] See Figure 1. While σ dimerization

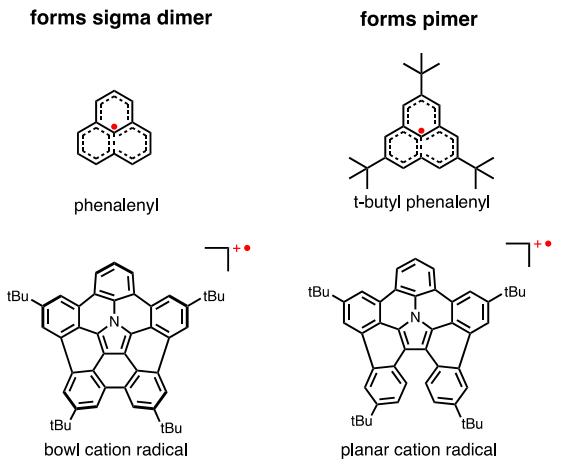

Figure 1. Examples of radicals that change the dimerization mode based on structural perturbations.[11]

is a standard bonding motif, the radical−radical bond within π dimers features a multicenter covalent bonding pattern that results from head-on π orbital overlap that results in the atoms being closer than van der Waals distance but much longer than a traditional two-atom bond.[11−16]

However, it remains difficult to understand and predict why some metastable radicals form σ dimers while others form pimers. It is important to develop models to predict why some radicals form σ dimers while others form pimers because the geometries and properties of the two types of radical dimers show striking differences. Optically, σ dimers absorb mostly UV light and have properties that are common to conventional closed-shell organic molecules. By contrast, π dimers usually absorb visible to near-infrared light and often show charge-transporting properties with broader energy bands than typical organic semiconductors.[15,16] Furthermore, σ dimers form predictable structures, often useful for dynamic covalent assemblies, while π dimers feature fluctuating torsional geometries about energetically flat minima on their potential energy surfaces. In contrast to normal "π stacked" closed-shell aromatics, the energetic minima for pimers are typically cofacial orientations to maximize orbital overlap rather than slip-stacked orientations.[15,16]

Recently, we developed a model based on examining the structural preferences of aryl dicyanomethyl radicals to understand the stereoelectronic principles that lead to some free radicals forming σ dimers while other structures form π dimers.[17] The conclusion from that study was that London dispersion forces, spin delocalization, and polarization play a

Received: September 14, 2021
Published: January 5, 2022

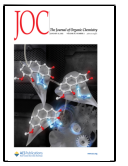

https://doi.org/10.1021/acs.joc.1c02246
J. Org. Chem. 2022, 87, 1507−1511

critical role in dictating whether a radical prefers to form a σ dimer or a π dimer. A limitation with that study was that it focused solely on electronic effects deriving from changing the *para* substituent and did not examine the effect of steric hindrance on the dimerization preference.

Previously, Seki and co-workers[16] showed that the julolidine-derived radical **3** forms a π dimer in both solution and the solid state. Here, we show that more sterically encumbered derivatives of **3**, radicals **1** and **2**,[18] form σ dimers (Figure 2). This steric-dependent dimerization behavior

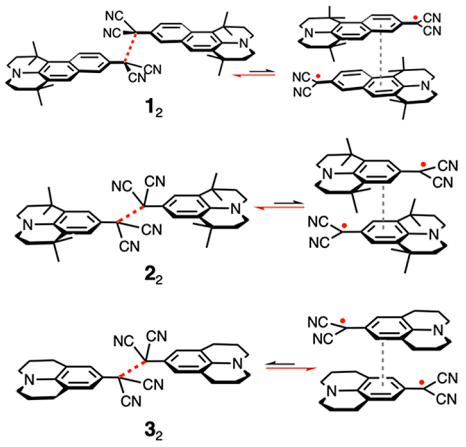

Figure 2. Equilibrium preferences for radicals **1**, **2**, and **3**.

contrasts with the behavior of other carbon-centered radicals, such as phenalenyl radicals,[14,19] where steric hindrance favors the π dimer over the σ dimer instead. Computational analysis indicates that steric hindrance disfavors the pimer by decreasing π orbital overlap and London dispersion forces in the pimer while having relatively little energetic effect on the σ dimer.

RESULTS AND DISCUSSION

Radicals **1** and **2** were synthesized by oxidation of the aryl dicyanomethane. The crystal structures (Figure 3) indicate that, in the solid state, they form σ dimers featuring an elongated σ bond. To evaluate the solution-phase preference, variable-temperature UV−vis experiments were conducted. Aryl dicyanomethyl radicals show bands in the visible to near-IR range of the optical spectrum. As the solution is cooled, dimers are formed, either a σ dimer or π dimer. The σ dimers and π dimers can be easily distinguished because π dimers maintain the radical absorption and feature a new broad absorption band in the near-IR ∼800 nm. Visually, the solutions typically become darker colored. In contrast, σ dimers absorb mostly in the UV region of the spectrum and are typically colorless or yellow. Radicals **1** and **2** are colored (orange and green, respectively) at room temperature but turn yellow upon cooling and the bands corresponding to the radical disappearance (**1**$_2$ is fluorescent). This indicates that, in the solution phase, **1** and **2** are also making σ dimers, similar to what we observe in the solid state.

Steric Hindrance Decreases Favorable Orbital Overlap and Dispersion in the Pimer. Why do the sterically encumbered derivatives **1** and **2** form σ dimers, while **3** forms a pimer? We considered several possibilities. First, changes in spin delocalization can affect dimerization preference, with highly delocalized spins favoring pimers, while more localized spins favoring σ dimers.[17] Second, steric hindrance could lead to a change in London dispersion forces between the pimers. Finally, steric hindrance could alter the overlap between the π orbitals in the pimer, leading to attenuated pimer stabilization by covalent bonding.

The computed spin densities are shown in Figure 4. Interestingly, while there are negligible differences between **2** and **3**, contrary to our expectation, the more conjugated derivative **1** has a more localized spin density than **2** or **3** (0.56

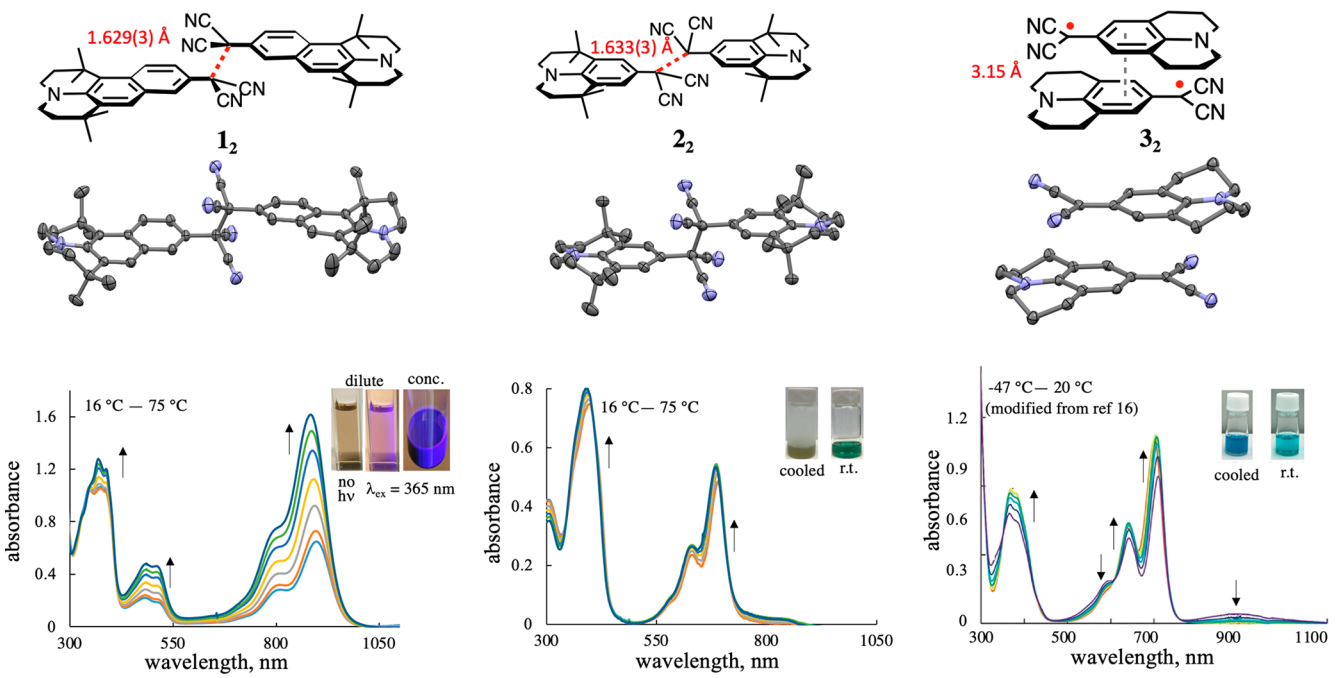

Figure 3. (top) Ortep at 50% thermal ellipsoids for **1**−**3**; (bottom) the variable-temperature UV−vis for **1**−**3**. The UV−vis and crystal structure for **3** are reproduced from prior work by Seki and co-workers,[16] while the others derive from the present work.

https://doi.org/10.1021/acs.joc.1c02246
J. Org. Chem. 2022, 87, 1507−1511

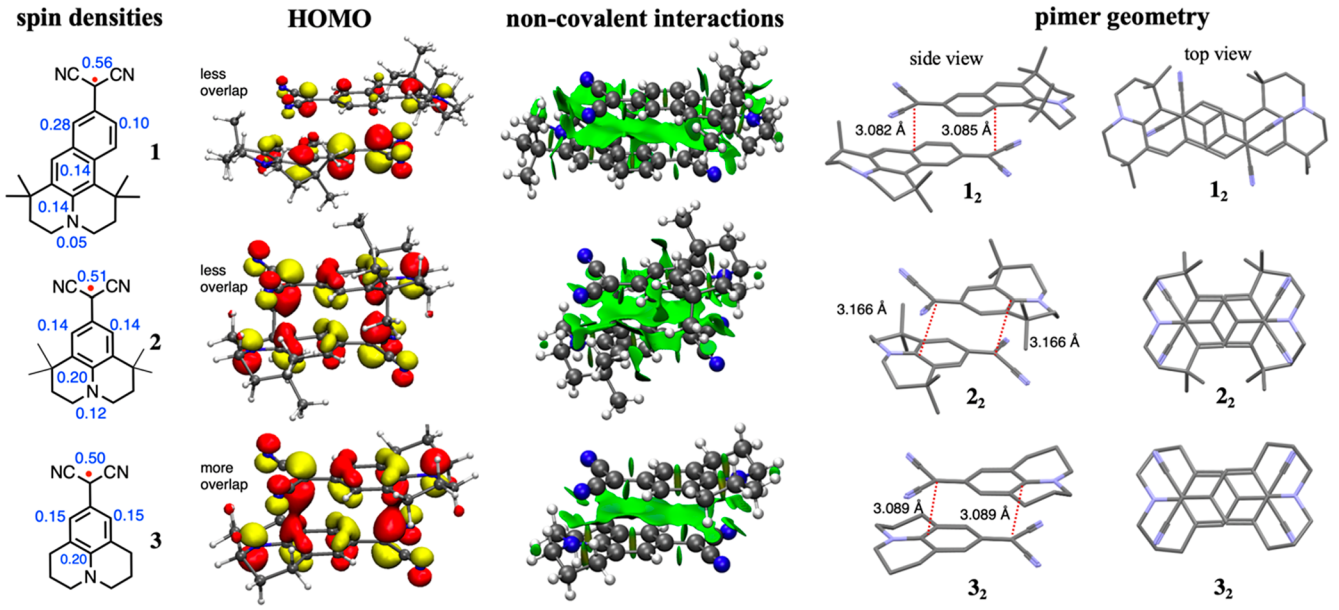

Figure 4. Select Mulliken spin densities (Uω-B97XD/6-31+G(d,p)) for **1**−**3**; the HOMO for **1**−**3** (Rω-B97XD/6-31+G(d,p), isovalue = 0.0375), the noncovalent interaction surface (Uω-B97XD/6-31+G(d,p), visualized with NCIPlot[20]), and the pimer geometry with select bond lengths (Rω-B97XD/6-31+G(d,p)).

spin density on benzylic carbon, compared to 0.51 and 0.50 for **2** and **3**, respectively). Apparently, the increased spatial separation of the donor nitrogen to the dicyanomethyl group makes it a less effective electron donor, and this is a more important effect than the increased conjugation opportunities provided by the naphthyl ring. Since the degree of delocalization correlates strongly with radical stability, it is not surprising that the equilibrium constant (K_a), determined from van 't Hoff plots, for **1** is larger than **2** (1.6×10^7 M^{-1} for **1** and 2.4×10^6 M^{-1} for **2**; see Supporting Information for van 't Hoff plots). Thus, changes in spin density could be a small effect for **1**, disfavoring the pimer relative to **2** and **3**, but cannot be a major effect for the change in dimerization mode between **2** and **3**.

What about changes in London dispersion forces[21,22] within the π dimers? Here, we plotted the noncovalent interaction surfaces[20] (Figure 4) and also computed the energetic differences between the σ and π dimer using two density functionals, one including a dispersion correction (B97D) and the other without (B98). The change in the ΔE is shown in Table 1. While these functionals are not useful for providing quantitative predictions of the equilibrium thermodynamics, the difference between the predictions gives an estimate of the relative importance of the dispersion energy. In all cases, the dispersion-corrected functional strongly favors the pimer and appears to overestimate the stabilities of the pimer. However, the $\Delta E_{dispersion}$, the difference between $\Delta E_{\sigma-\pi}$[23] at the B98 level and the $\Delta E_{\sigma-\pi}$ at the B97D level, gives an estimate of how much dispersion stabilizes the pimer in relative terms. Here, we find that the pimer dispersion energy follows the trend **1** > **3** > **2**. The greater dispersion **1** vs **3** can be understood by an increased surface area of interaction (see the noncovalent interactions surfaces in Figure 4), while the increased dispersion for **3** over **2** can be explained by the greater separation of the pimer for **2** than **3**. The computed pimer structures indicate that **2** is ~0.077 Å further separated than **3** because of the increased steric hindrance.

Table 1. Computed Equilibrium Energy Difference between the σ Dimer and Pimer for Radicals 1−3 and the Computed Grouped Mulliken Atomic Spin Density on the Benzylic Position (ω-B97XD/6-31+G(d,p))[a]

	$\Delta E_{\sigma-\pi}$ (kcal/mol)				
radicals	ω-B97XD	UB98	UB97D	$\Delta E_{dispersion}$	spin density
1	−1.9	−4.1	17.3	−21.4	0.56
2	−6.9	3.4	12.1	−8.7	0.51
3	8.3	8.7	26.9	−18.2	0.50

[a]A positive value for $\Delta E_{\sigma-\pi}$ indicates the pimer is favored.

Changes in covalent bonding could also explain why **3** favors a pimer over **2**. Inspecting the HOMOs for each pimer indicates less overlap of the π orbitals for **2** than **3**. This is also due to the radicals being further apart in the pimer of **2** over **3**. Thus, a combination of decreased stabilizing forces in the pimer from reduced orbital overlap and reduced dispersion forces because of the greater spatial separation of the radicals in this work explains the change in dimerization mode. Radical **1** is a difficult case; the pimer is favored by greater dispersion interactions because of a greater radical surface area than radicals **2** and **3**, but the σ dimer is overall energetically favored because of the more localized spin. Here, the σ dimer is computed to be the lowest energy form by 1.9 kcal/mol, suggesting that the more localized spin "wins out" over the greater pimer dispersion energy, but the σ dimer and pimer are computed to be nearly degenerate.

In conclusion, adding steric hindrance to these julolidine-derived dicyanomethyl radicals favors σ dimerization over π dimerization. This can be attributed to the increased steric hindrance in the pimer that leads to a more spatially separated radical−radical contact in the pimer, which reduces the favorable dispersion and covalent bonding forces. In contrast, the σ dimer is not affected significantly by the increased steric hindrance, which contrasts with other carbon-centered radicals, such as the phenalenyl radical, where steric hindrance perturbs the σ dimer more than the π dimer. On the other hand, the

https://doi.org/10.1021/acs.joc.1c02246
J. Org. Chem. 2022, 87, 1507−1511

effect of steric hindrance on the σ and π dimer is likely to be highly dependent on the structure of the radical and the pimer geometry. It is possible and perhaps likely that steric hindrance in different positions of aryl dicyanomethyl radicals will favor the pimer rather than the σ dimer. Support for this idea comes from a computation of the σ dimer−pimer energetics for a demethylated version of **1** that shows that the σ dimer is favored by 9.7 kcal/mol compared to the methylated derivative **1** being favored by 1.9 kcal/mol.

EXPERIMENTAL SECTION

General Methods. Nuclear magnetic resonance (^{1}H NMR and ^{13}C NMR) spectra were recorded on Agilent Varian MR-400 and Bruker NEO-400 instruments. NMR spectra were recorded in $CDCl_3$ at room temperature except where noted. EPR spectra were recorded on a Bruker FT-EPR instrument. UV−vis spectra were recorded on an Agilent 8453 spectrometer. Mass spectra were recorded on an Agilent QTOF 6540 instrument. The crystal structure was obtained on a BRUKER APEX II diffractometer equipped with an APEX II CCD detector. All reactions were performed under an argon atmosphere in oven-dried glassware. Xylenes were dried under activated molecular sieves (4 Å). All other chemical reagents were purchased from commercial sources and used without purification.

Synthesis Procedures. See Supporting Information (S3) for schemes and numbering.

6-Bromonaphthalen-2-amine (0.66 g, 3 mmol) and K_2CO_3 (1.38 g, 10 mmol) were dissolved in acetonitrile (10 mL) in a 50 mL round-bottom flask. 1-Bromo-3-methylbut-2-ene (1.20 g, 8 mmol) was added to the flask. The mixture was stirred at rt for 5 h. After completion, water was added to dissolve the salt, the solution was extracted with DCM, and the organic layer was concentrated under reduced pressure and purified by column chromatography on silica gel (R_f = 0.40, hexane/EtOAc = 20:1) to yield **1a** (0.91 g, 85%) as a yellow solid. ^{1}H NMR (400 MHz, chloroform-*d*): δ 7.79 (d, J = 1.9 Hz, 1H), 7.56 (d, J = 9.1 Hz, 1H), 7.46 (d, J = 8.8 Hz, 1H), 7.37 (dd, J = 8.8, 2.0 Hz, 1H), 7.10 (dd, J = 9.1, 2.6 Hz, 1H), 6.83 (d, J = 2.5 Hz, 1H), 5.25−5.21 (m, 2H), 3.95 (d, J = 6.3 Hz, 4H), 1.74 (s, 12H). ^{13}C {1H} NMR (101 MHz, $CDCl_3$): δ 147.3, 134.6, 133.6, 129.3, 129.2, 127.8, 127.7, 127.5, 121.3, 117.5, 114.6, 106.2, 48.3, 25.8, 18.0. HRMS (Q-TOF, ESI): m/z calcd for $C_{20}H_{24}BrN$, 358.1165 $[M + H]^+$; found, 358.1165.

For compound **1b**, compound **1a** (1.07 g, 3 mmol) was dissolved in ether (10 mL) in a 50 mL round-bottom flask at 0 °C, concentrated HCl (1 mL) was added to the solution, and the mixture was stirred at 0 °C for 20 min. Na_2SO_4 was added and filtered, and the solvent was removed under reduced pressure to give **1a**·HCl as a white solid. The solid was used without further purification. Methanesulfonic acid (10 mL, purged) and **1a**·HCl were mixed in a 50 mL round-bottom flask. The reaction was heated at 85 °C for 2 h under a N_2 atmosphere. After completion, ice was added to the flask, the solution was neutralized with ammonium hydroxide, then extracted with DCM, and the organic layer was concentrated under reduced pressure and purified by column chromatography on silica gel (R_f = 0.35, hexane/EtOAc = 20:1) to yield **1b** as a green solid (0.322 g, 30% yield). ^{1}H NMR (400 MHz, chloroform-*d*): δ 8.01 (d, J = 9.4 Hz, 1H), 7.76 (d, J = 2.3 Hz, 1H), 7.43 (s, 1H), 7.35 (dd, J = 9.4, 2.3 Hz, 1H), 3.28 (t, J = 6.1 Hz, 2H), 3.22−3.20 (m, 2H), 1.94−1.91 (m, 2H), 1.84−1.81 (m, 2H), 1.66 (s, 6H), 1.40 (s, 6H). ^{13}C {1H} NMR (101 MHz, $CDCl_3$): δ 141.0, 135.5, 130.4, 130.2, 129.1, 127.1, 126.6, 123.5, 120.0, 113.4, 47.6, 46.7, 42.3, 36.4, 33.2, 33.1, 30.9, 30.9. HRMS (Q-TOF, ESI): m/z calcd for $C_{20}H_{24}BrN$, 358.1165 $[M + H]^+$; found, 358.1164.

General Procedure to Couple Malononitrile to Aryl Bromide. NaOtBu (1.153 g, 12 mmol) was added into a 50 mL two-neck round-bottom flask, and 10 mL of xylene was added, followed by malononitrile (0.396 g, 6 mmol). The mixture was stirred at room temperature for 30 min. $Pd(PPh_3)_2Cl_2$ (0.070 g, 0.1 mmol) and **1b** (0.36 g, 1 mmol) were added to the solution, and the mixture was refluxed for 2 h. After cooling, brine (30 mL), DCM (30 mL), and Celite were added to the solution, filtered off, and extracted with DCM (30 mL × 3). The organic phase was dried over Na_2SO_4, filtered, and concentrated under reduced pressure. The obtained mixture was purified by silica gel column chromatography (R_f = 0.45, hexane/EtOAc = 8:2) to give the product as a red solid (0.16 g, 48%). ^{1}H NMR (400 MHz, chloroform-*d*): δ 8.23 (d, J = 9.1 Hz, 1H), 7.74 (d, J = 2.4 Hz, 1H), 7.55 (s, 1H),7.32−7.28 (m, 1H), 5.13 (s, 1H), 3.35−3.27 (m, 2H), 3.26−3.24 (m, 2H), 1.95−1.92 (m, 2H), 1.85−1.82 (m, 2H), 1.67 (s, 6H), 1.42 (s, 6H). ^{13}C{^{1}H} NMR (101 MHz, $CDCl_3$): δ 142.1, 136.0, 132.1, 127.7, 127.3, 126.8, 124.4, 121.7, 119.6, 116.6, 112.3, 47.5, 46.6, 42.1, 36.1, 33.2, 33.1, 30.8, 30.6, 28.0. HRMS (Q-TOF, ESI): m/z calcd for $C_{23}H_{25}N_3$, 342.1976 $[M - H]^-$; found, 342.1975.

For compound **2-H**, the bromide was prepared according to literature procedure.[18] The general procedure produced the dicyanomethane **2-H** as a green solid (0.12 g, 40%). ^{1}H NMR (400 MHz, chloroform-*d*): δ 6.92 (d, J = 8.2 Hz, 1H), 6.03 (d, J = 8.2 Hz, 1H), 4.50 (s, 1H), 3.12−3.09 (m, 2H), 3.06−3.03 (m, 2H), 1.83−1.76 (m, 4H), 1.46 (s, 6H), 1.28 (s, 6H). ^{13}C{^{1}H} NMR (101 MHz, $CDCl_3$): δ 153.1, 143.7, 124.9, 124.1, 116.6, 105.0, 47.6, 47.3, 40.6, 37.5, 32.4, 32.2, 29.2. HRMS (Q-TOF, ESI): m/z calcd for $C_{19}H_{23}N_3$, 292.1819 $[M - H]^-$; found, 292.1819.

General Procedure for Oxidation. In a 25 mL round-bottom flask, **1** (8 mg, 0.02 mmol) was dissolved in DCM (5 mL), and PbO_2 (30 mg, 0.13 mmol) was added. The mixture was stirred at rt for 15 min. The solid was filtered and washed with DCM, and then the filtrate was removed under reduced pressure to yield the radical/dimer.

Single-Crystal X-ray Structure Determination. Crystal structures are obtained with slow evaporation of a chloroform, 1,2-dichloroethane, and toluene solvent mixture. Intensity data were collected at 173 K using a Bruker Venture D8 (Cu Kα radiation) equipped with a microfocus sealed tube. Data reduction, multiscan absorption correction, structure solution, and refinement were performed using the APEX 3 software suite [Apex 3 Suite, Bruker AXS., Inc. Madison, Wisconsin, USA, 2020].

General Procedure for VT-UV−Vis Studies. The radical/dimer species were dissolved in toluene. The spectra were collected at 10 K increments with an equilibration time of 5 min for each temperature.

General Procedure for VT-EPR Studies. The 1−10 mM radical/dimer species toluene solution was purged and cannulated into an EPR tube. The EPR studies were then performed at 10 K increments with an equilibration time of 5 min for each temperature increment. The following instrument parameters were generally followed for each sample: modulation frequency, 100 kHz; receiver gain, 40 dB; modulation amplitude, 0.5; time constant, 0.01 ms; center field, 3355 G; sweep width, 150 G; microwave attenuation, 20 dB; number of data points, 2048; average number of scans, 4.

ASSOCIATED CONTENT

Supporting Information

The Supporting Information is available free of charge at https://pubs.acs.org/doi/10.1021/acs.joc.1c02246.

Compound characterization data, computational coordinates and absolute energies, and van 't Hoff plots (PDF)

Accession Codes

CCDC 2108897−2108898 contain the supplementary crystallographic data for this paper. These data can be obtained free of charge via www.ccdc.cam.ac.uk/data_request/cif, or by emailing data_request@ccdc.cam.ac.uk, or by contacting The Cambridge Crystallographic Data Centre, 12 Union Road, Cambridge CB2 1EZ, UK; fax: + 44 1223 336033.

https://doi.org/10.1021/acs.joc.1c02246
J. Org. Chem. 2022, 87, 1507−1511

AUTHOR INFORMATION

Corresponding Author

Arthur H. Winter − *Department of Chemistry, Iowa State University, Ames, Iowa 50010, United States;* orcid.org/0000-0003-2421-5578; Email: winter@iastate.edu

Authors

Rui Zhang − *Department of Chemistry, Iowa State University, Ames, Iowa 50010, United States*

Arkady Ellern − *Department of Chemistry, Iowa State University, Ames, Iowa 50010, United States*

Complete contact information is available at: https://pubs.acs.org/10.1021/acs.joc.1c02246

Funding

NSF CHE 2055335 and CHE 1764235

Notes

The authors declare no competing financial interest.

ACKNOWLEDGMENTS

We thank the Iowa State Chemical Instrumentation Facility, specifically Dr. Sarah Cady, for EPR guidance. We also are thankful for HPC@ISU equipment at Iowa State University, some of which have been purchased through funding provided by NSF under MRI grant no. CBS 1229081 and CRI grant no. 1205413.

REFERENCES

(1) Yang, X.-D.; Zhu, R.; Yin, J.-P.; Sun, L.; Guo, R.-Y.; Zhang, J. Bipyridinium-Bearing Multi-stimuli Responsive Chromic Material with High Stability. *Cryst. Growth Des.* **2018**, *18* (5), 3236−3243.

(2) Badía-Domínguez, I.; Peña-Álvarez, M.; Wang, D.; Pérez Guardiola, A.; Vida, Y.; Rodríguez González, S.; López Navarrete, J. T.; Hernández Jolín, V.; Sancho García, J. C.; García Baonza, V.; Nash, R.; Hartl, F.; Li, H.; Ruiz Delgado, M. C. Dynamic Covalent Properties of a Novel Indolo[3,2-b]carbazole Diradical. *Chemistry − A European Journal* **2021**, *27* (17), 5509−5520.

(3) Kobashi, T.; Sakamaki, D.; Seki, S. N-Substituted Dicyanomethylphenyl Radicals: Dynamic Covalent Properties and Formation of Stimuli-Responsive Cyclophanes by Self-Assembly. *Angew. Chem., Int. Ed.* **2016**, *55* (30), 8634−8638.

(4) Wang, D.; Capel Ferrón, C.; Li, J.; Gámez-Valenzuela, S.; Ponce Ortiz, R.; López Navarrete, J. T.; Hernández Jolín, V.; Yang, X.; Peña Álvarez, M.; García Baonza, V.; Hartl, F.; Ruiz Delgado, M. C.; Li, H. New Multiresponsive Chromic Soft Materials: Dynamic Interconversion of Short 2,7-Dicyanomethylenecarbazole-Based Biradicaloid and the Corresponding Cyclophane Tetramer. *Chemistry − A European Journal* **2017**, *23* (55), 13776−13783.

(5) Saha, M.; Bandyopadhyay, S. Stimuli Responsive Stable Radical Anion for Conductance Switching. *J. Phys. Chem. C* **2021**, *125* (11), 6427−6432.

(6) Geraskina, M. R.; Buck, A. T.; Winter, A. H. An Organic Spin Crossover Material in Water from a Covalently Linked Radical Dyad. *Journal of Organic Chemistry* **2014**, *79* (16), 7723−7727.

(7) Juetten, M. J.; Buck, A. T.; Winter, A. H. A radical spin on viologen polymers: organic spin crossover materials in water. *Chem. Commun.* **2015**, *51* (25), 5516−5519.

(8) Sakamaki, D.; Ghosh, S.; Seki, S. Dynamic covalent bonds: approaches from stable radical species. *Materials Chemistry Frontiers* **2019**, *3* (11), 2270−2282.

(9) Yuan, L.; Han, Y.; Tao, T.; Phan, H.; Chi, C. Formation of a Macrocycles-in-a-Macrocycle Superstructure with All-gauche Conformation by Reversible Radical Association. *Angew. Chem., Int. Ed.* **2018**, *57* (29), 9023−9027.

(10) Badía-Domínguez, I.; Pérez-Guardiola, A.; Sancho-García, J. C.; López Navarrete, J. T.; Hernández Jolín, V.; Li, H.; Sakamaki, D.; Seki, S.; Ruiz Delgado, M. C. Formation of Cyclophane Macrocycles in Carbazole-Based Biradicaloids: Impact of the Dicyanomethylene Substitution Position. *ACS Omega* **2019**, *4* (3), 4761−4769.

(11) (a) Mou, Z.; Uchida, K.; Kubo, T.; Kertesz, M. Evidence of σ- and π-Dimerization in a Series of Phenalenyls. *J. Am. Chem. Soc.* **2014**, *136* (52), 18009−18022. (b) Uchida, K.; Mou, Z.; Kertesz, M.; Kubo, T. *J Am. Chem. Soc.* ″Fluxional σ-Bonds of the 2,5,8-Trimethylphenalenyl Dimer: Direct Observation of the Sixfold σ-Bond Shift via a π-Dimer. *J. Am. Chem. Soc.* **2016**, *138* (13), 4665−4672. (c) Yokoi, H.; Hiroto, S.; Shinokubo, H. *J. Am. Chem. Soc.* ″Reversible σ-Bond Formation in Bowl-Shaped π-Radical Cations: The Effects of Curved and Planar Structures″. *J. Am. Chem. Soc.* **2018**, *140* (13), 4649−4655.

(12) Xiang, Q.; Guo, J.; Xu, J.; Ding, S.; Li, Z.; Li, G.; Phan, H.; Gu, Y.; Dang, Y.; Xu, Z.; Gong, Z.; Hu, W.; Zeng, Z.; Wu, J.; Sun, Z. Stable Olympicenyl Radicals and Their π-Dimers. *J. Am. Chem. Soc.* **2020**, *142* (25), 11022−11031.

(13) Xiang, Q.; Xu, J.; Guo, J.; Dang, Y.; Xu, Z.; Zeng, Z.; Sun, Z. Unveiling the Hidden σ-Dimerization of a Kinetically Protected Olympicenyl Radical. *Chemistry − A European Journal* **2021**, *27* (31), 8203−8213.

(14) Kubo, T. Synthesis, Physical Properties, and Reactivity of Stable, π-Conjugated, Carbon-Centered Radicals. *Molecules* **2019**, *24* (4), 665.

(15) Moshniaha, L.; Żyła-Karwowska, M.; Chmielewski, P. J.; Lis, T.; Cybińska, J.; Gońka, E.; Oschwald, J.; Drewello, T.; Rivero, S. M.; Casado, J.; Stępień, M. Aromatic Nanosandwich Obtained by σ-Dimerization of a Nanographenoid π-Radical. *J. Am. Chem. Soc.* **2020**, *142* (7), 3626−3635.

(16) Okino, K. a. H. S. a. I. Y. a. S. D. a. S. S. The Divergent Dimerization Behavior of N-Substituted Dicyanomethyl Radicals: Dynamically Stabilized versus Stable Radicals. *Angew. Chem., Int. Ed.* **2017**, *56* (52), 16597−16601.

(17) Peterson, J. P.; Ellern, A.; Winter, A. H. Spin Delocalization, Polarization, and London Dispersion Forces Govern the Formation of Diradical Pimers. *J. Am. Chem. Soc.* **2020**, *142* (11), 5304−5313.

(18) Merz, J.; Fink, J.; Friedrich, A.; Krummenacher, I.; Al Mamari, H. H.; Lorenzen, S.; Haehnel, M.; Eichhorn, A.; Moos, M.; Holzapfel, M.; Braunschweig, H.; Lambert, C.; Steffen, A.; Ji, L.; Marder, T. B. Pyrene Molecular Orbital Shuffle—Controlling Excited State and Redox Properties by Changing the Nature of the Frontier Orbitals. *Chemistry − A European Journal* **2017**, *23* (53), 13164−13180.

(19) Ratera, I.; Veciana, J. Playing with organic radicals as building blocks for functional molecular materials. *Chem. Soc. Rev.* **2012**, *41* (1), 303−349.

(20) Contreras-García, J.; Johnson, E. R.; Keinan, S.; Chaudret, R.; Piquemal, J.-P.; Beratan, D. N.; Yang, W. NCIPLOT: A Program for Plotting Noncovalent Interaction Regions. *J. Chem. Theory Comput.* **2011**, *7* (3), 625−632.

(21) Wagner, J. P.; Schreiner, P. R. London Dispersion in Molecular Chemistry—Reconsidering Steric Effects. *Angew. Chem., Int. Ed.* **2015**, *54* (42), 12274−12296.

(22) Geraskina, M. R.; Dutton, A. S.; Juetten, M. J.; Wood, S. A.; Winter, A. H. The Viologen Cation Radical Pimer: A Case of Dispersion-Driven Bonding. *Angew. Chem., Int. Ed.* **2017**, *56* (32), 9435−9439.

(23) Fischer, L. J.; Dutton, A. S.; Winter, A. H. Anomalous effect of non-alternant hydrocarbons on carbocation and carbanion electronic configurations. *Chemical Science* **2017**, *8* (6), 4231−4241.